Batteries & Supercaps

Research Article
doi.org/10.1002/batt.202200480

Chemistry Europe
European Chemical Societies Publishing

www.batteries-supercaps.org

Special Collection

Unraveling Factors Affecting Performance of Quinone-based Polymer Cathode in Aqueous Zinc-Ion Battery

Xiao Yang,[a, b] Yi Zhao,*[c] Qiuju Xu,[b] Xiangcheng Yuan,[b] and Jinzhang Liu*[b]

Organic cathode materials for aqueous rechargeable Zinc-ion batteries (ZIBs) include a large variety of aromatic molecules with redox-activity, and such polymer molecules vary largely in terms of specific capacity, discharge voltage plateau, and cycling stability. Here, three different quinone polymers are prepared by electropolymerizing dihydroxynaphthalene (DHN) isomers of 1,5-DHN, 1,6-DHN, and 1,7-DHN, respectively, and their energy storage performances in aqueous ZIBs are compared. Among the three cathode materials, the poly(1,6-DHN) cathode shows the best performance in specific capacity and cycling stability. The Zn||poly(1,6-DHN) cell shows a high areal capacity of 1.4 mAh cm^{-2} and a high capacity retention of 90% after 5000 cycles. By combing experiment with computation, the HOMO level of the polymer molecule is found to play a key role behind the specific capacity. Using the poly(1,7-DHN) cathode that suffers from faster capacity decay in the cycling process, our investigation suggests that residual ions stuck between molecular chains in the insertion/deinsertion process account for the capacity loss. This study provides a further understanding of organic cathode materials for aqueous ZIBs.

Introduction

The increasing demand of renewable energy sources like solar and wind has promoted the development of green energy systems. Because the power generation by solar panel or wind turbine is intermittent, an important supporting facility is the energy storage station. Lithium-ion batteries (LIBs) and sodium-sulfur batteries are primary candidates for large-scale energy storage, while these batteries contain flammable materials and suffer from fire risk.[1] Rechargeable aqueous Zn-ion batteries (ZIBs) have the advantage of high safety and low cost, owing to the intrinsic merits of Zn metal anode, such as high specific capacity (820 mAh g^{-1} or 5855 mAh cm^{-3}), bivalent Zn^{2+} as charge carrier, low reduction potential (−0.76 V vs. standard hydrogen electrode), and relatively higher abundance than Li in earth's crust.[2,3] In 2012, Xu et al. reported a rechargeable MnO_2||Zn battery using mild $ZnSO_4$ aqueous electrolyte.[4] Since then, many cathode materials based on metal compounds have been used as Zn^{2+} storage hosts.[5–7] These materials are generally crystalline, and the sluggish Zn^{2+} intercalation kinetics leads to poor power capability. Moreover, the repeatable insertion-deinsertion of ions could cause irreversible collapse of the crystal structure, which is responsible for the capacity decay of the cathode.

By comparison, organic electrode materials are much more diverse in type and molecular structure.[8] Many aromatic molecules containing carbonyl or amino groups, or both, are redox-active and can be combined with the Zn anode to make ZIBs. For instance, Chen et al. combined a calix[4]quinone (C4Q) based cathode and a Zn anode to make aqueous ZIB, which showed a discharge voltage plateau of 1 V.[9] Zhang et al. reported an organic molecular crystal based on 3,4,9,10-perylenetetracarboxylic dianhydride (PMC) for ultra-high rate Zn ion host.[10] Although their assembled Zn battery showed good power capability, the discharge median voltage was relatively low, as 0.5 V. The functional groups of redox-active aromatic polymers for charge storage are mainly carbonyl and amino groups. The amino-containing polymers such as polyaniline and poly(1,5-naphthalenediamine) as ZIB cathode materials are p-type and solely rely on the redox reactions at amino group sites.[11–13] Quinones as organic electrode materials belong to the n-type and are a big family. Quinone electrode materials have been applied in Li/Na-ion batteries using organic electrolytes.[14] When in aqueous electrolyte, the reversible conversion between hydroxyl and carbonyl groups are believed to be responsible for charge and discharge.[15] Although a large number of phenols can be polymerized into quinone polymers for making aqueous Zn-organic batteries, the clue is unclear for sorting out appropriate ones with good energy storage performance.[16,17]

Here, we look into factors affecting the energy storage performances of quinone polymers. For a comparison study, three dihydroxynaphthalene (DHN) isomers, named 1,5-DHN, 1,6-DHN, and 1,7-DHN were electropolymerized onto mesoporous activated carbon (AC) coatings for making ZIB cathodes. Particularly, the poly(1,6-DHN)/AC cathode was found to have the highest specific capacity and longest cycle life. When at a practical mass loading of 13.3 mg cm^{-2}, this cathode exhibited

[a] X. Yang
Wuhu State-Owned Factory of Machining
241007 Wuhu, Anhui Province (China)
[b] X. Yang, Dr. Q. Xu, Dr. X. Yuan, A/Prof. J. Liu
School of Materials Science and Engineering
Beihang University
100191 Beijing (China)
E-mail: ljz78@buaa.edu.cn
[c] Dr. Y. Zhao
State Key Laboratory of Chemical Engineering & College of Chemistry
Beijing University of Chemical Technology
100029 Beijing (China)
E-mail: zhaoyi91789@163.com

Supporting information for this article is available on the WWW under https://doi.org/10.1002/batt.202200480

Special Collection An invited contribution to a Special Collection on Organic Batteries.

Research Article
doi.org/10.1002/batt.202200480
Chemistry Europe
European Chemical Societies Publishing

an areal capacity of 1.36 mAh cm^{-2}, superior rate performance and excellent cycling stability (capacity retention of 90% after 5000 cycles). By combining experiment with theory, factors influencing the specific capacity and cycling stability of these representative quinones were investigated in detail.

Results and Discussion

The process for making a polymer/AC composite cathode is illustrated in Figure 1(a). Two optical photographs in Figure S1(c and d) show different colors of the electrolyte before and after the electropolymerization process, respectively. A scanning electron microscopy (SEM) image and an optical photograph of the carbon cloth are shown in the insets in Figure 1(a). SEM images of the bare AC coatign and the typical poly(1,6-DHN)/AC composite are shown in Figure 1(b) and (c), respectively. The AC granules are several micrometers in size and have a high specific surface area of 2280 m^2 g^{-1}, according to our BET analysis (Figure 1d). With the presence of electrodeposited poly(1,6-DHN), the originally smooth surfaces of AC granules were roughened, as shown in Figure 1(c). The AC coating that contains carbon black and polyvinyl difluoride as binder has a specific surface area of 1820 m^2 g^{-1}. After the electrodeposition of poly(1,6-DHN), the specific surface area of the poly(1,6-DHN)/AC composite was reduced to 350 m^2 g^{-1}. It is believed that the polymer molecules were not only deposited onto the outer surface, but also filled into the nanopores of AC granules. Raman spectra of the bare AC and the poly(1,6-DHN)/AC are compared in Figure S2. The newly emerged signals of C=C and C=O can be contributed by the electrodeposited poly(1,6-DHN).[16] Also, a Fourier transform infrared (FTIR) spectrum of the poly(1,6-DHN)/AC sample is shown in Figure S3. Signals of C=O. C–O, and C–H bonds can be observed. X-ray photoelectron spectroscopy (XPS) was employed to study the surface chemistry of the polymer-modified AC coating. In

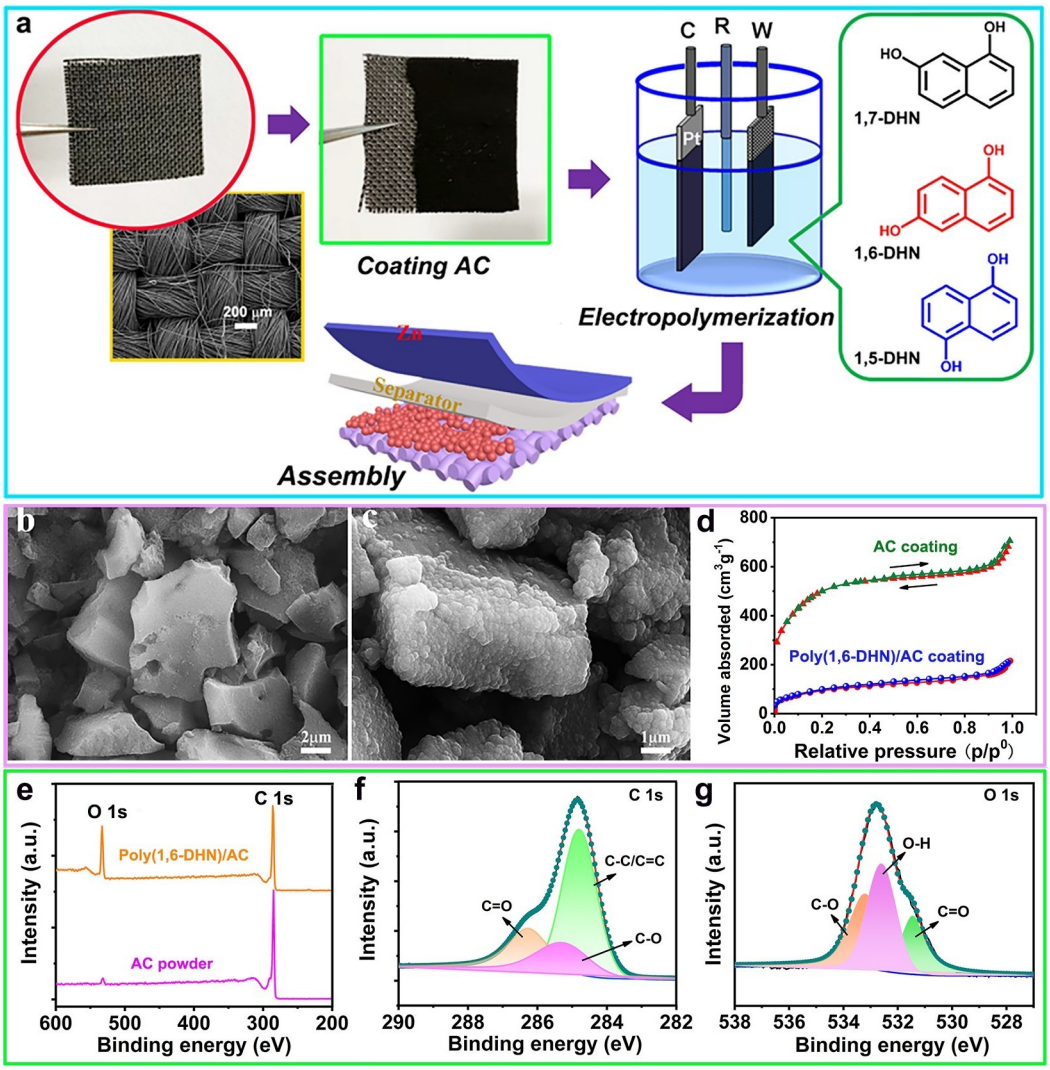

Figure 1. a) Illustration for the fabrication process of Zn-organic cells using poly(1,5-DHN)/AC, poly(1,6-DHN)/AC and poly(1,7-DHN)/AC cathodes, respectively. b) and c) SEM images of a bare AC coating and a poly(1,6-DHN)/AC coating, respectively. d) N_2 adsorption/desorption isotherms of the AC powder and the poly(1,6-DHN)/AC composite. e) Survey XPS spectra of AC and poly(1,6-DHN)/AC samples. f) and g) High-resolution C 1s and O 1s XPS spectra of the poly(1,6-DHN)/AC coating.

Research Article
doi.org/10.1002/batt.202200480
Chemistry Europe
European Chemical Societies Publishing

Figure 1(e), two survey XPS spectra collected from a poly(1,6-DHN)/AC coating and a bare AC coating are compared. The contents of oxygen in poly(1,6-DHN)/AC and bare AC are 18 and 3 atom%, respectively, given by our XPS analysis. The strong O signal from the poly(1,6-DHN)/AC sample can be attributed to oxygenated groups in the polymer. Figure 1(f and g) shows high-resolution C 1s and O 1s XPS spectra of the poly(1,6-DHN)/AC sample, respectively. Our deconvolution of the C 1s peak gives three sub-peaks assigned to C–C/C=C (284.6 eV), C=O (287.9 eV) and C–O (286.3 eV) bonds. Similarly, the O 1s peak is composed of three sub-peaks assigned to C=O, O–H, and C–O bonds. High-resolution C 1s and O 1s XPS spectra of the bare AC are shown in Figure S4(a) and (b), respectively. Compared with the bare AC, the poly(1,6-DHN)/AC contains much more C=O functional groups that would favour the electrochemical energy storage.

In order to sort out the optimal electrolyte for our organic cathodes, $ZnSO_4$, $ZnCl_2$, and $Zn(CF_3SO_3)_2$ solutions at an identical concentration of 2 M were used in the Zn-organic cell to collect cyclic voltammetry (CV) loops, as shown in Figure S5. The use of $ZnCl_2$ electrolyte leads to a narrower voltage window from 0.1 to 1.5 V. Both $Zn(CF_3SO_3)_2$ and $ZnSO_4$ electrolytes can extend the maximum voltage to 1.8 V, but the $ZnSO_4$ electrolyte renders the highest capacity. Hence, the 2 M $ZnSO_4$ electrolyte was used for the following studies.

Button-type Zn-organic cells were assembled using poly(1,5-DHN)/AC, poly(1,6-DHN)/AC, and poly(1,7-DHN)/AC as cathodes, respectively, and their CV loops at 5 mV s^{-1} are compared in Figure 2(a). For comparison, the CV loop of a Zn||AC hybrid supercapacitor is also shown. Note that the areal mass loadings of AC were identical for the four cells, as 2.8 mg cm^{-2}. The mass gains of electrodeposited poly(1,5-DHN), poly(1,6-DHN), and poly(1,7-DHN) were 1.5, 4.3, and 5.1 mg cm^{-2}, respectively. The enclosed area of a CV loop is related to the charge storage capacity. Apparently, the capacity of AC coating can be enhanced by introducing these redox-active polymers. Figure 2(b) shows galvanostatic charge-discharge (GCD) curves at 10 mA cm^{-2} collected from the four cells. The Zn||poly(1,6-DHN)/AC cell shows the highest areal capacity, which is nearly three times as large as that of the

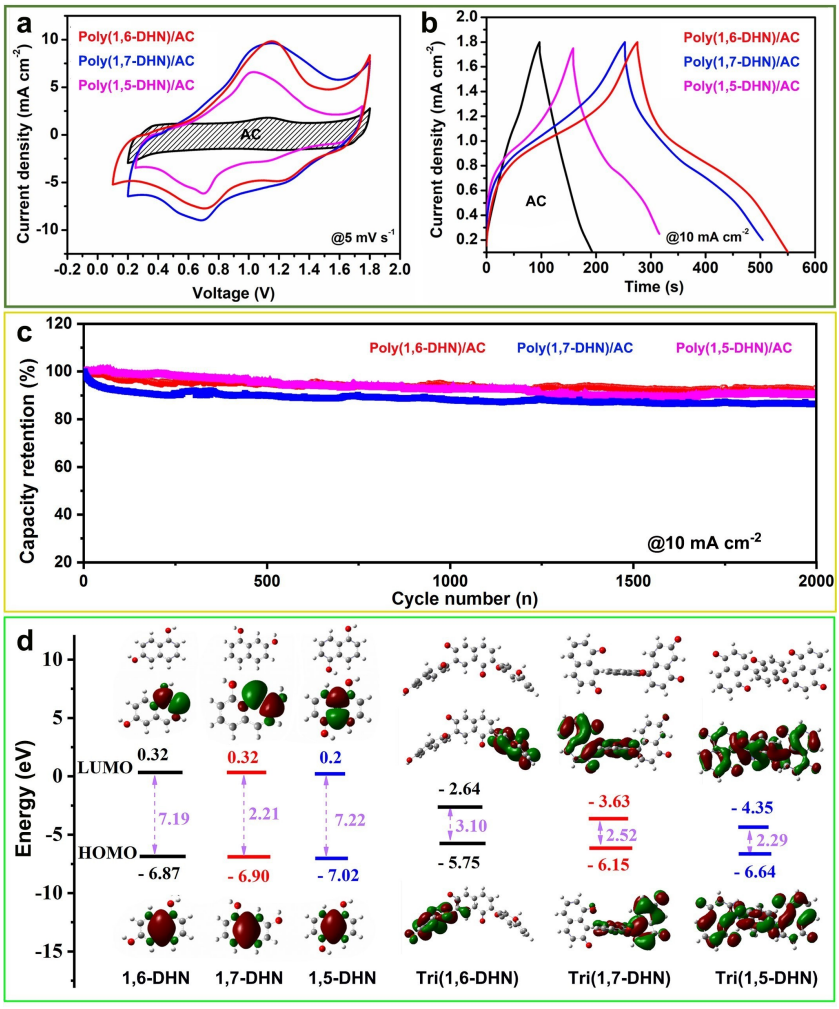

Figure 2. a) CV loops at 5 mV s^{-1} and b) GCD curves at 10 mA cm^{-2} of four Zn-ion cells using AC, poly(1,5-DHN)/AC, poly(1,6-DHN)/AC, and poly(1,7-DHN)/AC cathodes, respectively. c) Cycling performances of three Zn-ion cells using poly(1,5-DHN)/AC, poly(1,6-DHN)/AC, and poly(1,7-DHN)/AC cathodes, respectively. d) Calculate HOMO and LUMO levels for monomers and trimers of DHN molecules. The frontier molecular orbital diagrams of these molecules are shown.

Research Article
doi.org/10.1002/batt.202200480
Chemistry Europe
European Chemical Societies Publishing

Zn||AC cell. The poly(1,7-DHN) shows the poorest efficacy in boosting the capacity. In Figure 2b, long-term cycling performances of three cells using different polymer-modified AC cathodes are compared. After being continuously charged and discharged at 10 mA cm^{-2} for 2000 cycles, the capacity retentions of cells using poly(1,5-DHN)/AC, poly(1,6-DHN)/AC, and poly(1,6-DHN)/AC cathodes were 90%, 92%, and 86%, respectively. Therefore, the poly(1,6-DHN) shows the best performance in terms of areal capacity and cycling stability.

Dentisity Functional Theory (DFT) calculations were performed for monomers and trimers of the three different DHN molecules, which give the lowest unoccupied molecular orbital (LUMO) and the highest occupied molecular orbital (HOMO) levels, as displayed in Figure 2(d). Also, molecular structures and frontier molecular orbitals of these aromatic molecules are shown. The most possible molecular structures of three trimers, as shown in Figurer S6, were determined by DFT calculation, according to the lowest energy principle.[18] Normally, the LUMO level would be decreased and the HOMO level would be lifted up with increasing the polymerization degree, but these energy levels would be nearly stable if the polymerization degree is beyond 10.[19] For simplicity, here we use trimers to mimic the long-chain polymer molecules. It can be seen that the HOMO level of tri(1,6-DHN) is the highest among the three trimers. The HOMO level of tri(1,5-DHN) is the lowest, which can be correlated with the lowest specific capacity of poly(1,5-DHN). For the aqueous $ZnSO_4$ electrolyte, a general hydration model is that one Zn^{2+} would coordinate with 6 water molecules, as $[Zn–6H_2O)]^{2+}$.[20] Upon reaching the cathode, the charge transfer process can be regarded as hole transfer from the $[Zn–6H_2O)]^{2+}$ cluster to the HOMO level of the polymer molecule, followed by the collapse of the hydration structure. The LUMO and HOMO levels of $[Zn–6H_2O)]^{2+}$ were calculated to be −0.24 and −0.67 eV, respectively. Therefore, the energy barrier between HOMO levels of poly(1,6-DHN) and $[Zn–6H_2O)]^{2+}$ is the lowest, which facilitates the acceptation of Zn^{2+} by the polymer cathode.

To gain insights into the capacity decay of our quinone cathode in the cycling process, the poly(1,7-DHN)/AC cathode that has the poorest cycling stability was used in this study. Two poly(1,7-DHN)/AC cathodes were cycled at 5 mA cm^{-2} in button-type Zn-ion cells for 100 and 2000 cycles, and their capacity retentions were 92% and 83%, respectively. The two cycled cathodes were removed from the cell and washed using diluted HCl solution to dissolve byproducts over the surface, and then thoroughly rinsed using deionized water. Figure 3(a) shows survey XPS spectra of the poly(1,7-DHN) after 100 and 2000 cycles. Our XPS analysis gives the contents of residual S that is contributed by inserted SO_4^{2-} in the cycled polymer cathodes. As a result, the poly(1,7-DHN) after 100 and 2000 cycles contained 0.55 and 0.62 at% sulfur. A trend is that, the longer the cycling process, the more capacity loss and the higher S content in the polymer, as shown in Figure 3(b). The capacity of a redox-active polymer is determined by the amount of carbonyl groups that participate in the redox reaction. Since the molecular chains were entangled in the polymer, a tiny amount of Zn^{2+} and SO_4^{2-} could be stuck

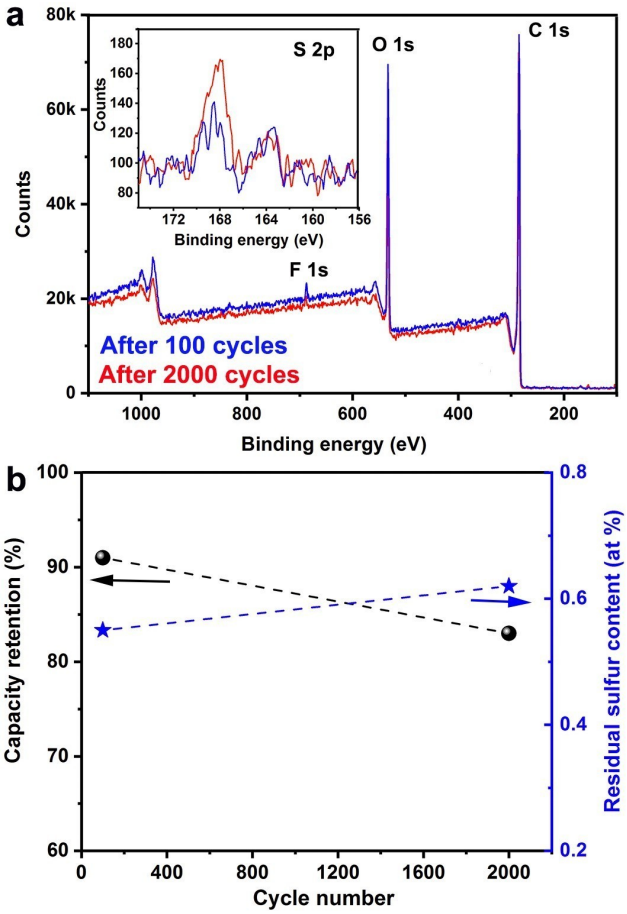

Figure 3. a) Survey XPS spectra of two poly(1,7-DHN)/AC cathode after being cycled in ZIB cells for 100 and 2000 cycles, respectively. The insert shows high-resolution S 2p spectra. b) Capacity retentions and sulfur contents in the two cycled cathodes.

between molecular chains in the charge-discharge process, thus blocking paths for following ion insertion and extraction in the polymer.[16] Some carbonyl groups along the ion diffusion path would be unreachable by inserted ions for redox reactions, resulting in capacity loss of the cathode.

Now the electrochemical behaviors of the poly(1,6-DHN)/AC cathode are investigated. For a group of Zn||poly(1,6-DHN)/AC cells with different AC mass loadings in the cathode, their rate performances tested from 1 to 20 mA cm^{-2} are shown in Figure 4(a). The higher the mass loading of AC coating, the more the mass gain of electrodeposited poly(1,6-DHN) and the higher the areal capacity. For the poly(1,6-DHN)/AC cathode with overall mass loading of 13.3 mg cm^{-2} (including AC and poly(1,6-DHN)), a high areal capacity of 1.37 mAh cm^{-2} was achieved. When the current was increased from 1 to 20 mA cm^{-2}, the capacity of this cathode was decreased from 1.37 to 0.93 mAh cm^{-2}, corresponding to a capacity retention of 68%. The gravimetric specific capacities of poly(1,6-DHN)/AC cathodes with different overall mass loadings were obtained, as shown in Figure S7. A maximum specific capacity was 117 mAh g^{-1}, corresponding to the areal mass loading of 6.86 mg cm^{-2}, as shown in Table S1. For the cell with total mass

Research Article
doi.org/10.1002/batt.202200480
Chemistry Europe
European Chemical Societies Publishing

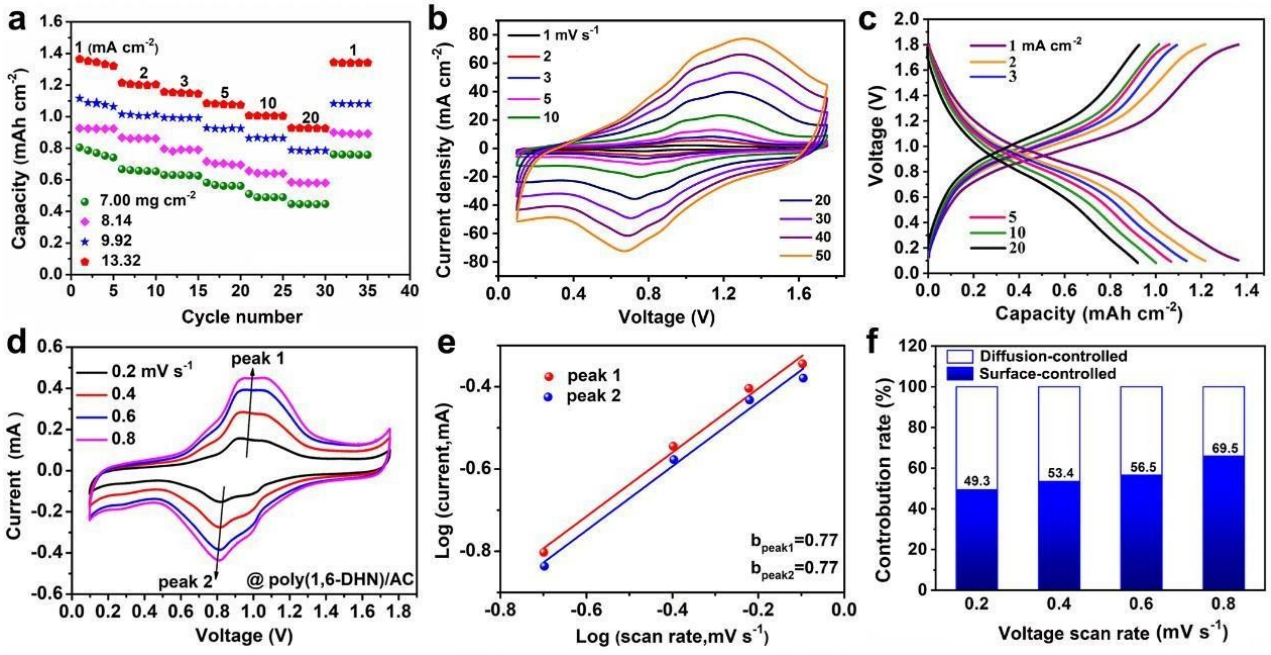

Figure 4. a) Rate performances of Zn||poly(1,6-DHN)/AC cells with different overall mass loadings in the cathode. b) CV loops and c) GCD curves of the Zn||poly(1,6-DHN)/AC cell with mass loading of 13.3 mg cm^{-2} in the cathode. d) CV curves of the cell at slow voltage scan rates. e) Linear fittings for deducing b-values at different voltage scan rates. f) Contribution percentages of diffusion-controlled and surface-controlled charge storage processes.

loading of 13.3 mg cm^{-2} in the cathode, its CV loops at different voltage scan rates and GCD curves at different current densities are shown in Figure 4(b and c), respectively. To understand the charge storage mechanism, CV loops at low voltage scan rates were collected, as shown in Figure 4(d). For oxidation and reduction peaks over the CV curve, the relationship between peak current I and the voltage scan rate ν can be written as $i = a\nu^b$, where a and b are adjustable parameters.[20] When the b-value is 1, it suggests a surface-controlled capacitive process. When the b-value is 0.5, the charge storage is via a diffusion-controlled process that is similar to the LIB. Using the oxidation (peak 1) and reduction (peak 2) peaks in Figure 4(d), the b-value is deduced to be 0.77, as shown in Figure 4(e). Hence, the charge storage by our poly(1,6-DHN)/AC cathode is through a hybrid process. The peak current can also be written as $I = k_1\nu + k_2\nu^{0.5}$, where k_1 and k_2 represent the fractions of surface-controlled and diffusion-controlled processes, respectively. Accordingly, the contribution percentages of the two charge-storage process are deduced, as shown in Figure 4(f). The surface-controlled pseudo-capacitive process takes 49.3% when at 0.2 mV s^{-1}, and it is increased to 65.9% when at 0.8 mV s^{-1}. It means the diffusion-controlled process was gradually suppressed with increasing the voltage scan rate. This can be understood that, when at a faster voltage scan rate, the time as well as depth of Zn^{2+} insertion into the polymer cathode are reduced, thus making the surface-controlled capacitive process dominant.

Ex-situ XPS spectra were collected from the poly(1,6-DHN)/AC cathode at charged (1.8 V) and discharged (0.1 V) states, as shown in Figure 5(a). The Zn signal from the cathode at discharged state is stronger than that at charged state. Figure 5(b) shows two high-resolution Zn 2p XPS spectra collected from the cathode at charged and discharged states, respectively. Also, high-resolution O 1s XPS spectra from the cathode at charged and discharged states are compared in Figure 5c. According to our peak deconvolution, the signal of carbonyl group in the charged polymer is stronger than that at discharged state. Figure 5d and e show SEM images of the poly(1,6-DHN)/AC cathode at charged and discharged states, respectively. Corresponding to the areas in SEM images of the two samples, elemental mappings given by the energy dispersive X-ray spectroscopy are presented. Strong C and O signals were emerged from this cathode at either charged or discharged states.

Normally, the flake-shaped byproduct identified as $Zn_4SO_4(OH)_6 \cdot 5H_2O$ would be emerged over the cathode surface in the discharging process.[13,19] However, these flakes can be dissolved in the charging process, leaving subtle amount of Zn and S in the cathode surface. The dissolution of byproduct flakes could be resulted from the change of pH value at the interface between cathode and electrolyte, because H^+ also participates in the charge/discharge process.[16] Now Figure 5(f) is used to illustrate the energy storage process. Both H^+ and Zn^{2+} can be inserted into the cathode in the discharge process. To further investigate the accurate capacity contribution of inserted H^+, we analysed the percentages of C=O, –OH, and C–O–Zn groups in poly(1,6-DHN)AC cathode during discharging process, as shown in Table S2. Along with the inserted Zn^{2+} and H^+, the C=O groups can be converted into O–H and C–O–Zn groups. Hence, the capacity contribution of inserted H+ is estimated to be 47.1%. The inserted Zn^{2+} ion can be coordinated by two neighboring carbonyl groups. One inserted

Research Article
doi.org/10.1002/batt.202200480
Chemistry Europe
European Chemical Societies Publishing

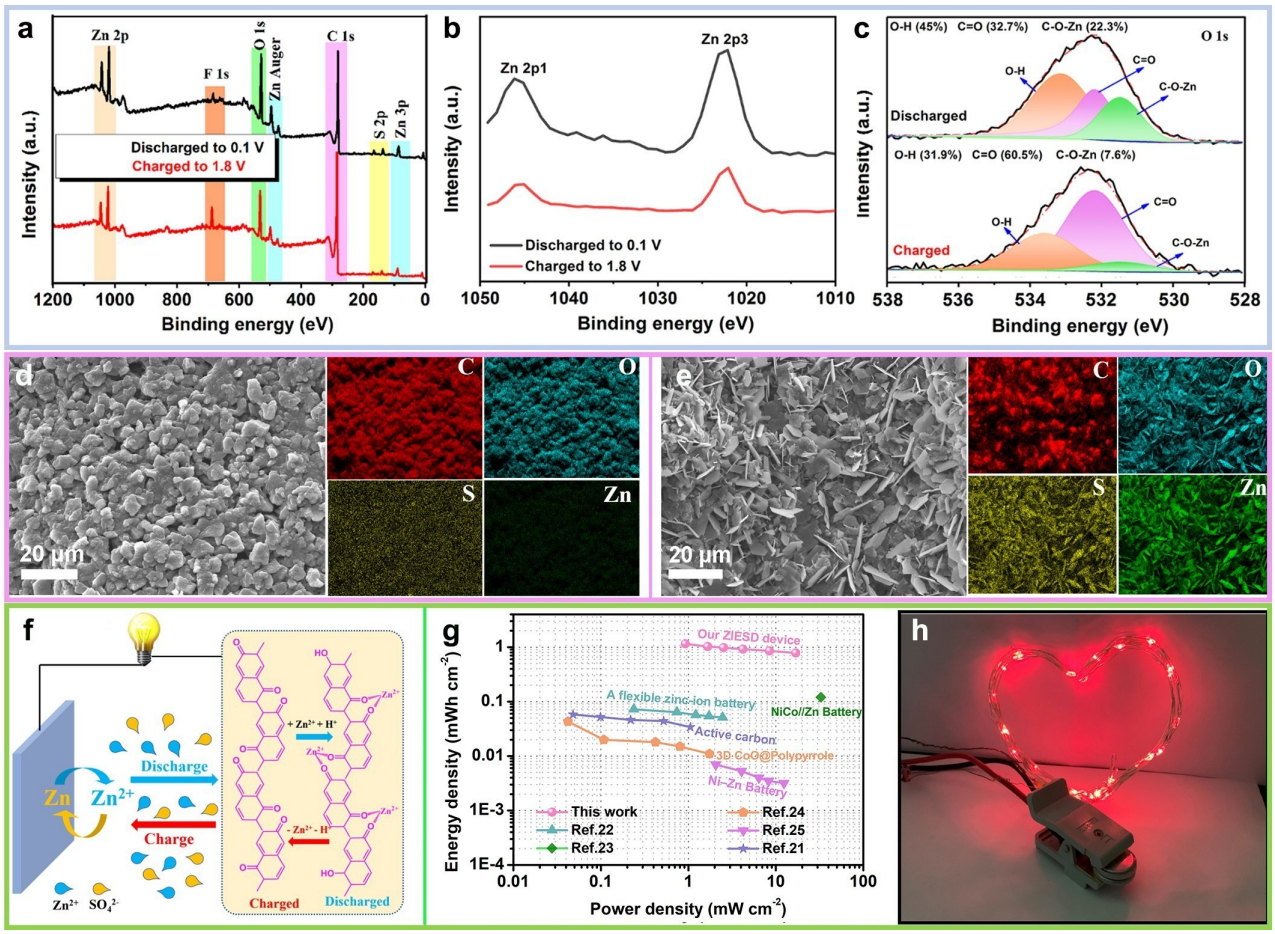

Figure 5. a) Survey XPS survey spectra of the poly(1,6-DHN)/AC cathode at charged and discharged states. b) High-resolution Zn 2p and c) O 1s XPS spectra of the poly(1,6-DHN)/AC cathode at charged and discharged states, respectively. d) and e) SEM images and corresponding elemental mappings of the poly(1,6-DHN)/AC cathode at charged and discharged states, respectively. f) Illustration for the charge/discharge process of the Zn//poly(1,6-DHN)/AC cell. g) Ragone plot showing density *and* power densities of our ZIB. Data for other cells are also shown. h) Optical photograph showing two Zn//poly(1,6-DHN)/AC cells in series connection for lighting up a string of red LEDs.

H^+ would combine with a single carbonyl group to form the hydroxyl group. In the charge process, Zn^{2+} and H^+ ions are extracted from the cathode, and the released H^+ ions cause the dissolution of byproduct flakes.

For the Zn||poly(1,6-DHN)/AC cell with a maximum areal capacity of 1.37 mAh cm^{-2}, the areal energy density is calculated to be 1.15 mWh cm^{-2} by using the discharge median voltage of 0.84 V. The corresponding power density is calculated to be 0.92 mW cm^{-2}. The Ragone plot of this cell is shown in Figure 5(g). For comparison, energy and power densities of other devices are marked as well, including flexible aqueous rechargeable Zn-ion battery,[22] yarn-based NiCo||Zn textile battery,[23] AC||Zn hybrid supercapacitor,[21] 3D CoO@Polypyrrole electrode,[24] and Ni–Zn battery.[25] As a demonstration of practical application, a string of light-emission diodes were lit up by two button-type Zn||poly(1,6-DHN)/AC cells in series connection. In addition, GCD curves collected from two pouch-type Zn||poly(1,6-DHN)/AC cells in parallel and in series connections are shown in Figure S8(a) and (b), respectively. It can be seen that the capacity was doubled up by the series connection.

Conclusion

In summary, three different quinone polymers were prepared using 1,5-DHN, 1,6-DHN, and 1,7-DHN isomers, respectively, and were combined with Zn anodes to make aqueous ZIBs for studying factors linking to the energy storage performances of quinone-type cathode materials. These AC-supported polymer cathodes varied in specific capacity and cycling stability, and the poly(1,6-DHN)/AC cathode was found to have the best performance. By combing experiment with theoretical calculation, it is found that a higher HOMO level of the polymer molecule can bring out a higher specific capacity. Using the poly(1,7-DHN) cathode that was inferior in cycling life, compared to the other two counterparts, a trend was unveiled that the longer the cycling process, the larger the capacity loss and the more residual SO_4^{2-} ions in the polymer. It implies that a small fraction of inserted ions could be stuck between molecular chains in the polymer, thus blocking paths for ion diffusion and causing the capacity decay. The Zn||poly(1,6-DHN)/AC cell showed a high areal capacity of 1.4 mAh cm^{-2} and excellent cycling stability, as the capacity retention was 90%

after 5000 cycles. Also, it showed a high energy density of 1.15 mWh cm^{-2}. This study provides a further understanding of the energy storage performances of polymer cathode materials for ZIBs.

Experimental Section

Materials preparation

AC powder (YP-80, Kuraray Co.) and carbon fabric (WOS1009, CeTech. Co.) were purchased from the market. The monomers of 1,5-DHN, 1,6-DHN, and 1,7-DHN were purchased from Aladdin Co., China. All chemicals were of analytical grade and used without further purification. The three poly(DHN)/AC cathodes are prepared using an electrochemical polymerization method, which is similar to our previous studies.[26,27] First, a mixture slurry was prepared by dispersing AC powder, carbon black, and polyvinylidene fluoride as binder at a weight ratio of 8:1:1 into N-methylpyrrolidone solvent. Second, the slurry was coated onto a piece of carbon fiber cloth, followed by a drying process at 60 °C for 12 h. Third, the AC-coated carbon cloth was used as work electrode in a three-electrode cell containing a mixture solution of 0.01 M 1,6-DHN molecules and 1 M H_2SO_4 for conducting the electropolymerization process. Using an Ag/AgCl reference electrode and a Pt foil counter electrode, the poly(1,6-DHN) was electrodeposited onto the AC coating by running CV test at 20 mV s^{-1} within the voltage range from −0.4 to 1.2 V for 50 cycles (Figure S1). Finally, the poly(1,6-DHN)/AC electrode was removed out and rinsed with deionized water, followed by a drying process in a vacuum oven at 80 °C overnight. Other cathodes named as poly(1,5-DHN)/AC and poly(1,7-DHN)/AC were prepared in a similar way by using 1,5-DHN and 1,7-DHN monomers, respectively.

Electrochemical measurements

Button-type cells were made for testing the electrochemical performances of aqueous ZIBs. For instance, a poly(1,6-DHN)/AC cathode, a glass fiber membrane soaked with 2 M Zn_2SO_4 electrolyte, and a 80-μm-thick Zn foil anode were stacked and sealed in a CR2032 coin cell. An electrochemical workstation (CS350) and a LAND battery testing system (CT3001A) were used for electrochemical tests.

Materials characterization

The morphology and structure of the electrodes were investigated using Scanning electron microscopy SEM (SUPRA55). X-ray photoelectron spectroscopy photoelectron spectroscopy (XPS, Thermo Scientific Escalab 250Xi) were taken to analysis the elemental composition and valence states of the cathodes. Brunauer–Emmett–Teller (BET) analyzer (ASAP 2460) was used to characterize the specific surface area of electrodes. Besides, Raman spectrum were collected by a Raman spectrometer (Renishaw inVia) using a 532 nm laser. While proceeding the ex-situ XPS test, the ex-situ samples were prepared by tuning the cathodes to full charged and discharged potentials and then washed with distilled water for few times, followed by drying water in a vacuum oven at 80 °C for 24 h.

Computational details.

The Gaussian 09 software package was used for all calculations. The solvation model SMD and meta GGA density functional M06 with the 6-31 + G(d,p) all electron basis set and ultrafine integration grids were used to optimize the structures of the DHN molecules before and after polymerization. The calculations were performed with a 5×5×2 supercell for the three DHN isomers.[28] To obtain the optimized structures, the forces on all atoms were minimized to be smaller than 0.01 eV/Å.

Acknowledgements

This work was financially supported by The National Natural Science Foundation of China (NSFC, Grant No. 22179003, 22209006).

Conflict of Interest

The authors declare no conflict of interest.

Data Availability Statement

Research data are not shared.

Keywords: quinone-based polymer · cathode · aqueous zinc-ion battery

[1] A. Castillo, D. F. Gayme, *Energy Convers. Manage.* **2014**, *87*, 885–894.
[2] J. Liu, C. Xu, Z. Chen, S. Ni, Z. X. Shen, *Green Energy & Environ.* **2018**, *3*, 20–41.
[3] M. Song, H. Tan, D. Chao, H. J. Fan, *Adv. Funct. Mater.* **2018**, *28*, 1802564.
[4] C. Xu, B. Li, H. Du, F. Kang, *Angew. Chem. Int. Ed.* **2012**, *51*, 933–935; *Angew. Chem.* **2012**, *124*, 957–959.
[5] B. Tang, J. Zhou, G. Fang, F. Liu, C. Zhu, C. Wang, A. Pan, S. Liang, *J. Mater. Chem. A* **2019**, *7*, 940–945.
[6] L. Wang, J. Zheng, *Materials Today Advances* **2020**, *7*, 100078.
[7] S. Bi, H. Wang, R. Wang, *Z. Niu, 2D Mater.* **2022**, *9*, 042001.
[8] T. B. Schon, B. T. McAllister, P. Li, D. S. Seferos, *Chem. Soc. Rev.* **2016**, *45*, 6345–6404.
[9] Q. Zhao, W. Huang, Z. Luo, L. Liu, Y. Lu, Y. Li, L. Li, J. Hu, H. Ma, J. Chen, *Sci. Adv.* **2018**, *4*, eaao1761.
[10] H. Z. Zhang, Y. Fang, F. Yang, X. Liu, X. Lu, *Energy Environ. Sci.* **2020**, *13*, 2515–2513.
[11] H. Y. Shi, Y. J. Ye, K. Liu, Y. Song, X. Sun, *Angew. Chem. Int. Ed.* **2018**, *57*, 16359–16363; *Angew. Chem.* **2018**, *130*, 16597–16601.
[12] F. Wan, L. Zhang, X. Wang, S. Bi, Z. Niu, J. Chen, *Adv. Funct. Mater.* **2018**, *28* 1804975.
[13] Y. Zhao, Y. Wang, Z. Zhao, J. Zhao, T. Xin, N. Wang, J. Liu, *Energy Storage Mater.* **2020**, *28*, 64–72.
[14] Y. Wu, R. Zeng, J. Nan, D. Shu, Y. Qiu, S. L. Chou, *Adv. Energy Mater.* **2017**, *7*, 1700278.
[15] E. J. Son, J. H. Kim, K. Kim, C. B. Park, *J. Mater. Chem. A* **2016**, *4*, 11179–11202.
[16] Y. Zhao, Y. X. Huang, F. Wu, R. J. Chen, L. Li, *Mater. Horiz.* **2021**, *8*, 3124–3132.
[17] K. W. Nam, H. Kim, Y. Beldjoudi, T.-W. Kwon, D. J. Kim, J. F. Stoddart, *J. Am. Chem. Soc.* **2020**, *142*, 2541–2548.
[18] R. Salcedo, M. Salmón, M. Aguilar, T. Hernández-Perez, M. Saloma, *Polymer* **2001**, *42*, 8737–8742.
[19] Y. Zhao, X. X. Wang, T. Xin, N. Wang, J. Z. Liu, *Sustain. Energy Fuels* **2019**, *3*, 3603–3610.
[20] N. Díaz, D. Suárez, K. M. Merz Jr, *Chem. Phys. Lett.* **2000**, *326*, 288–292.
[21] L. Dong, X. Ma, Y. Li, L. Zhao, W. Liu, J. Cheng, C. Xu, B. Li, Q. H. Yang, F. Kang, *Energy Storage Mater.* **2018**, *13*, 96–102.

[22] Q. Zhang, C. Li, Q. Li, Z. Pan, J. Sun, Z. Zhou, B. He, P. Man, L. Xie, L. Kang, X. Wang, J. Yang, T. Zhang, P. P. Shum, Q. Li, Y. Yao, L. Wei, *Nano Lett.* **2019**, *19*, 4035–4042.
[23] Y. Huang, W. S. Ip, Y. Y. Lau, J. Sun, J. Zeng, N. S. Yeung, W. S. Ng, H. Li, Z. Pei, Q. Xue, Y. Wang, J. Yu, H. Hu, C. Zhi, *ACS Nano* **2017**, *11*.
[24] C. Zhou, Y. Zhang, Y. Li, J. Liu, *Nano Lett.* **2013**, *13*, 2078–2085.
[25] Y. Zeng, Y. Meng, Z. Lai, X. Zhang, M. Yu, P. Fang, M. Wu, Y. Tong, X. Lu, *Adv. Mater.* **2017**, *29*, 1702698.
[26] T. Xin, Y. Wang, N. Wang, H. Li, Z. Zhang, J. Liu, *J. Mater. Chem. A* **2019**, *7*, 23976–2.
[27] Y. Zhao, Y. X. Huang, F. Wu, R. J. Chen, L. Li, *Adv. Mater.* **2021**, *33*, 2106469.
[28] Y. C. Fan, Y. Zhao, S. Li, Y. Liu, Y. Lv, Y. Zhu, R. Xiang, S. Maruyama, H. Zhang, Q. F. Zhang, *J. Energy Chem.* **2021**, *59*, 63–68.

Manuscript received: November 6, 2022
Revised manuscript received: December 21, 2022
Accepted manuscript online: December 26, 2022
Version of record online: January 13, 2023